Antibody evasion by SARS-CoV-2 Omicron subvariants BA.2.12.1, BA.4, and BA.5

Qian Wang[1*], Yicheng Guo[1*], Sho Iketani[1,2], Manoj S. Nair[1], Zhiteng Li[1], Hiroshi Mohri[1], Maple Wang[1], Jian Yu[1], Anthony D. Bowen[1,3], Jennifer Y. Chang[3], Jayesh G. Shah[3], Nadia Nguyen[1], Zhiwei Chen[4], Kathrine Meyers[1,3], Michael T. Yin[1,3], Magdalena E. Sobieszczyk[1,3], Zizhang Sheng[1], Yaoxing Huang[1], Lihong Liu[1#], and David D. Ho[1,2,3#]

[1]Aaron Diamond AIDS Research Center, Columbia University Vagelos College of Physicians and Surgeons, New York, NY, USA.

[2]Department of Microbiology and Immunology, Columbia University Vagelos College of Physicians and Surgeons, New York, NY, USA.

[3]Division of Infectious Diseases, Department of Medicine, Columbia University Vagelos College of Physicians and Surgeons, New York, NY, USA.

[4]AIDS Institute and Department of Microbiology, Li Ka Shing Faculty of Medicine, The University of Hong Kong, Pokfulam, Hong Kong Special Administrative Region, People's Republic of China.

*Equal contribution

[#]Address correspondence to Lihong Liu (ll3411@cumc.columbia.edu) or David D. Ho (dh2994@cumc.columbia.edu), Columbia University Vagelos College of Physicians and Surgeons, 701 W. 168th Street, New York, NY 10032, USA.

Abstract

SARS-CoV-2 Omicron subvariants BA.2.12.1 and BA.4/5 have surged dramatically to become dominant in the United States and South Africa, respectively[1,2]. These novel subvariants carrying additional mutations in their spike proteins raise concerns that they may further evade neutralizing antibodies, thereby further compromising the efficacy of COVID-19 vaccines and therapeutic monoclonals. We now report findings from a systematic antigenic analysis of these surging Omicron subvariants. BA.2.12.1 is only modestly (1.8-fold) more resistant to sera from vaccinated and boosted individuals than BA.2. However, BA.4/5 is substantially (4.2-fold) more resistant and thus more likely to lead to vaccine breakthrough infections. Mutation at spike residue L452 found in both BA.2.12.1 and BA.4/5 facilitates escape from some antibodies directed to the so-called class 2 and 3 regions of the receptor-binding domain[3]. The F486V mutation found in BA.4/5 facilitates escape from certain class 1 and 2 antibodies but compromises the spike affinity for the viral receptor. The R493Q reversion mutation, however, restores receptor affinity and consequently the fitness of BA.4/5. Among therapeutic antibodies authorized for clinical use, only bebtelovimab retains full potency against both BA.2.12.1 and BA.4/5. The Omicron lineage of SARS-CoV-2 continues to evolve, successively yielding subvariants that are not only more transmissible but also more evasive to antibodies.

Main text

Severe acute respiratory syndrome coronavirus 2 (SARS-CoV-2) Omicron or B.1.1.529 variant continues to dominate the coronavirus disease 2019 (COVID-19) pandemic. Globally, the BA.2 subvariant has rapidly replaced previous subvariants BA.1 and BA.1.1 (Fig. 1a). The recent detection and dramatic expansion of three new Omicron subvariants have raised concerns. BA.2.12.1 emerged in the United States in early February and expanded substantially (Fig. 1a), now accounting for over 55% of all new SARS-CoV-2 infections in the country[2]. BA.4 and BA.5 emerged in South Africa in January and rapidly became dominant there with a combined frequency of over 88%[4]. These new Omicron subvariants have been detected worldwide, with a combined frequency of over 50% in recent weeks. However, their growth trajectories in the U.S. and South Africa indicate a significant transmission advantage that will likely result in further expansion, as is being observed in countries such as the United Kingdom (Fig. 1a). Phylogenetically, these new subvariants evolved independently from BA.2 (Fig. 1b). The spike protein of BA.2.12.1 contains L452Q and S704L alterations in addition to the known mutations in BA.2, whereas the spike proteins of BA.4 and BA.5 are identical, each with four additional alterations: Del69-70, L452R, F486V, and R493Q, a reversion mutation (Fig. 1c). The location of several of these mutations within RBD of the spike protein raises the specter that BA.2.12.1 and BA.4/5 may have evolved to further escape from neutralizing antibodies.

Neutralization by monoclonal antibodies

To understand antigenic differences of BA.2.12.1 and BA.4/5 from previous Omicron subvariants (BA.1, BA.1.1, and BA.2) and the wild-type SARS-CoV-2 (D614G), we produced each pseudovirus and then assessed the sensitivity of each pseudovirus to neutralization by a panel of 21 monoclonal antibodies (mAbs) directed to known neutralizing epitopes on the viral spike. Among these, 19 target the four epitope classes in the receptor binding domain (RBD)[3], including REGN10987 (imdevimab)[5], REGN10933 (casirivimab)[5], COV2-2196 (tixagevimab)[6], COV2-2130 (cilgavimab)[6], LY-CoV555 (bamlanivimab)[7], CB6 (etesevimab)[8], Brii-196 (amubarvimab)[9], Brii-198 (romlusevimab)[9], S309 (sotrovimab)[10], LY-CoV1404 (bebtelovimab)[11], ADG-2[12], DH1047[13], S2X259[14], CAB-A17[15] and ZCB11[16], as well as 1-20, 2-15, 2-7[17] and 10-40[18] from our group. Two other mAbs, 4-18 and 5-7[17], target the N-terminal domain (NTD). Our findings are shown in Fig. 2a, as well as in Extended Data Figs. 1 and 2. Overall, 18 and 19 mAbs lost

neutralizing activity completely or partially against BA.2.12.1 and BA.4/5, respectively. Neutralization profiles were similar for BA.2 and BA.2.12.1 except for three class 3 RBD mAbs (Brii-198, REGN10987, and COV2-2130) that were either inactive or further impaired against the latter subvariant. Compared to BA.2 and BA.2.12.1, BA.4/5 showed substantially greater neutralization resistance to two class 2 RBD mAbs (ZCB11 and COV2-2196) as well as modest resistance to two class 3 RBD mAbs (REGN10987 and COV2-2130). Collectively, these differences suggest that mutations in BA.2.12.1 confer greater evasion from antibodies to class 3 region of RBD, whereas mutations in BA.4/5 confer greater evasion from antibodies to class 2 and class 3 regions. Only four RBD mAbs (CAB-A17, COV2-2130, 2-7, and LY-COV1404) retained good in vitro potency against both BA.2.12.1 and BA.4/5 with IC_{50} below 0.1 μg/mL. Importantly, among these four mAbs, COV2-2130 (cilgavimab) is one component of a combination known as Evusheld that is authorized for prevention of COVID-19, while only LY-COV1404 or bebtelovimab is authorized for therapeutic use in the clinic. For antibody combinations previously authorized or approved for clinical use, all showed a substantial loss of activity in vitro against BA.2.12.1 and BA.4/5. As for a mAb directed to the antigenic supersite of N-terminal domain (NTD)[19], 4-18 lost neutralizing activity against all Omicron subvariants. A mAb to the NTD alternate site, 5-7[20], was also inactive against BA.2.12.1 and BA.4/5 but retained modest activity against BA.1 and BA.1.1 (Fig. 2a).

A subset of the pseudovirus neutralization data was confirmed for four monoclonal antibodies (COV2-2196, ZCB11, REGN10987, and LY-CoV1404) in neutralization experiments using authentic viruses BA.2 and BA.4 (Extended Data Figs. 1b and 2b). Similar neutralization patterns were observed in the two assays, although the precise 50% neutralizing titers were different.

To identify the mutations in BA.2.12.1 and BA.4/5 that confer antibody resistance, we assessed the neutralization sensitivity of pseudoviruses carrying each of the point mutations in the background of D614G or BA.2 to the aforementioned panel of mAbs and combinations. Detailed findings are presented in Extended Data Figs. 3, 4, and 5, and most salient results are highlighted in Fig. 2b and discussed here. Substitutions (M, R, and Q) at residue L452, previously found in the Delta and Lambda variants[21,22], conferred resistance largely to classes 2 and 3 RBD mAbs, with L452R being the more detrimental mutation. F486V broadly impaired the neutralizing

activity of several class 1 and 2 RBD mAbs. Notably, this mutation decreased the potency of ZCB11 by >2000-fold. In contrast, the reversion mutation R493Q sensitized BA.2 to neutralization by several class 1 and 2 RBD mAbs. This finding is consistent with our previous study[23] showing that Q493R found in the earlier Omicron subvariants mediated resistance to the same set of mAbs. L452, F486, and Q493, situated at the top of RBD, are among the residues most commonly targeted by SARS-CoV-2 neutralizing mAbs whose epitopes have been defined (Fig. 2c). In silico structural analysis showed that both L452R and L452Q caused steric hindrance to the binding by class 2 RBD mAbs. One such example is shown for LY-CoV555 (Fig. 2d), demonstrating the greater clash because of the arginine substitution and explaining why this particular mutation led to a larger loss of virus-neutralizing activity (Fig. 2b). Structural modeling of the F486V again revealed steric hindrance to binding by class 2 RBD mAbs such as REGN10933, LY-CoV555, and 2-15 caused by the valine substitution (Fig. 2e).

Receptor affinity

Epidemiological data clearly indicate that both BA.2.12.1 and BA.4/5 are very transmissible (Fig. 1a); however, the additional mutations at the top of RBD (Fig. 2c) of these subvariants raises the possibility of a significant loss of affinity for the viral receptor, human angiotensin-converting enzyme 2 (hACE2). We therefore measured the binding affinity of purified spike proteins of D614G and major Omicron subvariants to dimeric hACE2 using surface plasmon resonance (SPR). The spike proteins of the Omicron subvariants exhibited similar binding affinities to hACE2, with K_D values ranging from 1.66 nM for BA.4/5 to 2.36 nM for BA.2.12.1 to 2.79 nM for BA.1.1 (Fig. 3a). Impressively, despite having $\geq$17 mutations in the RBD including some that mediate antibody escape, BA.2.12.1 and BA.4/5 also evolved concurrently to gain a slightly higher affinity for the receptor than an ancestral SARS-CoV-2, D614G (K_D 5.20 nM).

To support the findings by SPR and to probe the role of point mutations in hACE2 binding, we tested BA.2, BA.2.12.1, and BA.4/5 pseudoviruses, as well as pseudoviruses containing key mutations, to neutralization by dimeric hACE2 in vitro. The 50% inhibitory concentration (IC_{50}) values were lower for BA.4/5 and BA.2.12.1 than that of BA.2 (Fig. 3b), again indicating that these two emerging Omicron subvariants have not lost receptor affinity. Our results also showed that the F486V mutation compromised receptor affinity, as previously reported[24], while the R493Q

reversion mutation improved receptor affinity. To structurally interpret these results, we modeled F486V and R493Q mutations based on the crystal structure of BA.1-RBD-hACE2 complex[25] overlaid with ligand-free BA.2 RBD (PDB: 7U0N and 7UB0). This analysis found that both R493 and F486 are conformationally similar between BA.1 and BA.2, and F486V led to a loss of interaction with a hydrophobic pocket in hACE2 (Fig. 3c). On the other hand, the R493Q reversion mutation restored a hydrogen bond with H34 and avoided the charge repulsion by K31, seemingly having the opposite effect of F486V. Interestingly, the mutation frequency at F486 had been exceedingly low (<10E-5) until the emergence of BA.4/5 (Extended Data Table 1), probably because of a compromised receptor affinity. Taken together, our findings in Figs. 2 and 3 suggest that F486V allowed BA.4 and BA.5 to extend antibody evasion while R493Q compensated to regain fitness in receptor binding.

Neutralization by polyclonal sera

We next assessed the extent of BA.2.12.1 and BA.4/5 resistance to neutralization by sera from four different clinical cohorts. Sera from persons immunized with only two doses of COVID-19 mRNA vaccines were not examined because most of them could not neutralize earlier Omicron subvariants[23,26]. Instead, we measured serum neutralizing activity for persons who received three shots of mRNA vaccines (boosted), individuals who received mRNA vaccines before or after non-Omicron infection, and patients with either BA.1 or BA.2 breakthrough infection after vaccination. Their clinical information is described in Extended Data Table 2, and the serum neutralization profiles are presented in Extended Data Fig. 6 and the 50% inhibitory dose (ID_{50}) titers are summarized in Fig. 4a. For the "boosted" cohort, neutralization titers were noticeably lower (4.6-fold to 6.2-fold) for BA.1, BA.1.1, and BA.2 compared to D614G (Fig. 4b), as previously reported[23,26]. Titers for BA.2.12.1 and BA.4/5 were even lower, by 8.1-fold and 19.2-fold, respectively, relative to D614G, and by 1.8-fold and 4.2-fold, respectively, relative to BA.2. A similar trend was observed for serum neutralization for the other cohorts, with the lowest titers against BA.4/5, followed next by titers against BA.2.12.1. Relative to BA.2, BA.2.12.1 and BA.4/5 showed 1.2-fold to 1.4-fold and 1.6-fold to 4.3-fold, respectively, greater resistance to neutralization by sera from these individuals who had both mRNA vaccination and SARS-CoV-2 infection. In addition, sera from vaccinated and boosted individuals were assayed for

neutralization of authentic viruses (Extended Data Figs. 6e and 6f). Neutralization titers for BA.4 were 2.7-fold lower on average compared to titers for BA.2, in line with the pseudovirus results.

We also conducted serum neutralization assays on pseudoviruses containing point mutations found in BA.2.12.1 or BA.4/5 in the background of BA.2. Del69-70, L452M/R/Q, and F486V each modestly (1.1-fold to 2.4-fold) decreased the neutralizing activity of sera from all cohorts, while the R493Q reversion mutation modestly (~1.5-fold) enhanced the neutralization (Fig. 4c and Extended Data Fig. 7). S704L, a mutation close to the S1/S2 cleavage site, did not appreciably alter the serum neutralization titers against BA.2. For "boosted" serum samples, the impact of each point mutant on neutralization resistance was quantified and summarized in Fig. 4b.

Using these serum neutralization results, we then constructed a graphic display to map antigenic distances among D614G, various Omicron subvariants, and individual point mutants using only results from the "boosted" serum samples to avoid confounding effects from differences in clinical histories in the other cohorts. Utilizing methods well established in influenza research[27], all virus and serum positions on the antigenic map were optimized so that the distances between them correspond to the fold drop in neutralizing ID_{50} titer relative to the maximum titer for each serum. Each unit of distance in any direction on the antigenic map corresponds to a two-fold change in ID_{50} titer. The resultant antigenic cartography (Fig. 4d) shows that BA.1, BA.1.1, and BA.2 are approximately equidistant from the "boosted" sera, with each about 2-3 antigenic units away. BA.2.12.1 is further away from BA.2 by about 1 antigenic unit. Most strikingly, BA.4/5 is 4.3 antigenic units further from "boosted" sera than D614G, and 2 antigenic units further than BA.2. Each of the point mutants Del69-70, L452M/Q/R, and F486V adds antigenic distance from these sera compared to BA.2 and D614G, whereas R493Q has the opposite effect. Overall, this map makes clear that BA.4/5 is substantially more neutralization resistant to sera obtained from boosted individuals, with several mutations contributing to the antibody evasion.

Discussion

We have systematically evaluated the antigenic properties of SARS-CoV-2 Omicron subvariants BA.2.12.1 and BA.4/5, which are rapidly expanding globally (Fig. 1a). It is apparent that BA.2.12.1 is only modestly (1.8-fold) more resistant to sera from vaccinated and boosted

172 individuals than the BA.2 subvariant that currently dominates the global pandemic (Figs. 4b). On
173 the other hand, BA.4/5 is substantially (4.2-fold) more resistant, a finding consistent with results
174 recently posted by other groups[1,28]. This antigenic distance is similar to that between the Delta
175 variant and the ancestral virus[29] and thus is likely to lead to more breakthrough infections in the
176 coming months. A key question now is whether BA.4/5 would out-compete BA.2.12.1, which
177 poses less of an antigenic threat. This competition is now playing out in the United Kingdom.
178 These new Omicron subvariants were first detected there almost simultaneously in late March of
179 2022. However, BA.2.12.1 now accounts for 13% of new infections in the U.K., whereas the
180 frequency is over 50% for BA.4/5 (Fig. 1a), suggesting a transmission advantage for the latter.

181

182 Epidemiologically, since both of these two Omicron subvariants have a clear advantage in
183 transmission, it is therefore not surprising that their abilities to bind the hACE2 receptor remain
184 robust (Fig. 3a) despite numerous mutations in the spike protein. In fact, BA.4/5 may have slightly
185 higher affinity for the receptor, consistent with suggestions that it might be more fit[30]. However,
186 assessment of transmissibility would be more revealing by conducting studies on BA.2.12.1 and
187 BA.4/5 in animal models[31].

188

189 Our studies on the specific mutations found in BA.2.12.1 and BA.4/5 show that Del69-70,
190 L452M/R/Q, and F486V could individually contribute to antibody resistance, whereas R493Q
191 confers antibody sensitivity (Fig. 4b). Moreover, the data generated using SARS-CoV-2-
192 neutralizing mAbs suggest that a mutation at L452 allows escape from class 2 and class 3 RBD
193 antibodies and that the F486V mutation mediates escape from class 1 and class 2 RBD antibodies
194 (Fig. 2b). It is not clear how Del69-70, a mutation that might increase infectivity[32] and previously
195 seen in the Alpha variant[33], contributes to antibody resistance except for the possible evasion from
196 certain neutralizing antibodies directed to the NTD. As for the use of clinically authorized mAbs
197 to treat or block infection by BA.2.12.1 or BA.4/5, only bebtelovimab (LY-COV1404)[11] retains
198 exquisite potency while the combination of tixagevimab and cilgavimab (COV2-2196 and COV2-
199 2130)[6] shows a modest loss of activity (Fig. 2a).

200

As the Omicron lineage has evolved over the past few months (Fig. 1b), each successive subvariant has seemingly become better and better at human transmission (Fig. 1a) as well as in antibody evasion[23,34]. It is only natural that scientific attention remains intently focused on each new subvariant of Omicron. However, we must be mindful that each of the globally dominant variants of SARS-CoV-2 (Alpha, Delta, and Omicron) emerged stochastically and unexpectedly. Vigilance in our collective surveillance effort must be sustained.

References

1 Khan, K. *et al.* Omicron sub-lineages BA.4/BA.5 escape BA.1 infection elicited neutralizing immunity. *medRxiv*, doi:10.1101/2022.04.29.22274477 (2022).

2 Centers for Disease Control and Prevention. *COVID Data Tracker*, <https://covid.cdc.gov/covid-data-tracker/#variant-proportions> (2022).

3 Barnes, C. O. *et al.* SARS-CoV-2 neutralizing antibody structures inform therapeutic strategies. *Nature* **588**, 682-687, doi:10.1038/s41586-020-2852-1 (2020).

4 Shu, Y. & McCauley, J. GISAID: Global initiative on sharing all influenza data - from vision to reality. *Euro Surveill* **22**, doi:10.2807/1560-7917.ES.2017.22.13.30494 (2017).

5 Hansen, J. *et al.* Studies in humanized mice and convalescent humans yield a SARS-CoV-2 antibody cocktail. *Science* **369**, 1010-1014, doi:10.1126/science.abd0827 (2020).

6 Zost, S. J. *et al.* Potently neutralizing and protective human antibodies against SARS-CoV-2. *Nature* **584**, 443-449, doi:10.1038/s41586-020-2548-6 (2020).

7 Jones, B. E. *et al.* The neutralizing antibody, LY-CoV555, protects against SARS-CoV-2 infection in nonhuman primates. *Sci Transl Med* **13**, doi:10.1126/scitranslmed.abf1906 (2021).

8 Shi, R. *et al.* A human neutralizing antibody targets the receptor-binding site of SARS-CoV-2. *Nature* **584**, 120-124, doi:10.1038/s41586-020-2381-y (2020).

9 Ju, B. *et al.* Human neutralizing antibodies elicited by SARS-CoV-2 infection. *Nature* **584**, 115-119, doi:10.1038/s41586-020-2380-z (2020).

10 Pinto, D. *et al.* Cross-neutralization of SARS-CoV-2 by a human monoclonal SARS-CoV antibody. *Nature* **583**, 290-295, doi:10.1038/s41586-020-2349-y (2020).

11 Westendorf, K. *et al.* LY-CoV1404 (bebtelovimab) potently neutralizes SARS-CoV-2 variants. *Cell Rep* **39**, 110812, doi:10.1016/j.celrep.2022.110812 (2022).

12 Rappazzo, C. G. *et al.* Broad and potent activity against SARS-like viruses by an engineered human monoclonal antibody. *Science* **371**, 823-829, doi:10.1126/science.abf4830 (2021).

13 Li, D. *et al.* In vitro and in vivo functions of SARS-CoV-2 infection-enhancing and neutralizing antibodies. *Cell* **184**, 4203-4219 e4232, doi:10.1016/j.cell.2021.06.021 (2021).

14 Tortorici, M. A. *et al.* Broad sarbecovirus neutralization by a human monoclonal antibody. *Nature* **597**, 103-108, doi:10.1038/s41586-021-03817-4 (2021).

15 Sheward, D. J. *et al.* Structural basis of Omicron neutralization by affinity-matured public antibodies. *bioRxiv*, doi:10.1101/2022.01.03.474825 (2022).

16 Zhou, B. *et al.* An elite broadly neutralizing antibody protects SARS-CoV-2 Omicron variant challenge. *bioRxiv*, doi:10.1101/2022.01.05.475037 (2022).

17 Liu, L. *et al.* Potent neutralizing antibodies against multiple epitopes on SARS-CoV-2 spike. *Nature* **584**, 450-456, doi:10.1038/s41586-020-2571-7 (2020).

18 Liu, L. *et al.* An antibody class with a common CDRH3 motif broadly neutralizes sarbecoviruses. *Sci Transl Med*, eabn6859, doi:10.1126/scitranslmed.abn6859 (2022).

19 Cerutti, G. *et al.* Potent SARS-CoV-2 neutralizing antibodies directed against spike N-terminal domain target a single supersite. *Cell Host Microbe* **29**, 819-833 e817, doi:10.1016/j.chom.2021.03.005 (2021).

20 Cerutti, G. *et al.* Neutralizing antibody 5-7 defines a distinct site of vulnerability in SARS-CoV-2 spike N-terminal domain. *Cell Rep* **37**, 109928, doi:10.1016/j.celrep.2021.109928 (2021).

21 Planas, D. *et al.* Reduced sensitivity of SARS-CoV-2 variant Delta to antibody neutralization. *Nature* **596**, 276-280, doi:10.1038/s41586-021-03777-9 (2021).

22 Kimura, I. *et al.* The SARS-CoV-2 Lambda variant exhibits enhanced infectivity and immune resistance. *Cell Rep* **38**, 110218, doi:10.1016/j.celrep.2021.110218 (2022).

23 Liu, L. *et al.* Striking antibody evasion manifested by the Omicron variant of SARS-CoV-2. *Nature* **602**, 676-681, doi:10.1038/s41586-021-04388-0 (2022).

24 Starr, T. N. *et al.* Shifting mutational constraints in the SARS-CoV-2 receptor-binding domain during viral evolution. *bioRxiv*, doi:10.1101/2022.02.24.481899 (2022).

25 Geng, Q. *et al.* Structural Basis for Human Receptor Recognition by SARS-CoV-2 Omicron Variant BA.1. *J Virol* **96**, e0024922, doi:10.1128/jvi.00249-22 (2022).

26 Iketani, S. *et al.* Antibody evasion properties of SARS-CoV-2 Omicron sublineages. *Nature* **604**, 553-556, doi:10.1038/s41586-022-04594-4 (2022).

27 Smith, D. J. *et al.* Mapping the antigenic and genetic evolution of influenza virus. *Science* **305**, 371-376, doi:10.1126/science.1097211 (2004).

28 Tuekprakhon, A. *et al.* Antibody escape of SARS-CoV-2 Omicron BA.4 and BA.5 from vaccine and BA.1 serum. *Cell*, doi:https://doi.org/10.1016/j.cell.2022.06.005 (2022).

29 Rössler, A. *et al.* BA.2 omicron differs immunologically from both BA.1 omicron and pre-omicron variants. *medRxiv*, doi:10.1101/2022.05.10.22274906 (2022).

30 Cao, Y. *et al.* BA.2.12.1, BA.4 and BA.5 escape antibodies elicited by Omicron infection. *Nature*, doi:10.1038/s41586-022-04980-y (2022).

31 Munoz-Fontela, C. *et al.* Animal models for COVID-19. *Nature* **586**, 509-515, doi:10.1038/s41586-020-2787-6 (2020).

32 Chen, Y. *et al.* Emerging SARS-CoV-2 variants: Why, how, and what's next? *Cell Insight* **1**, 100029, doi:https://doi.org/10.1016/j.cellin.2022.100029 (2022).

33 Wang, R. *et al.* Analysis of SARS-CoV-2 variant mutations reveals neutralization escape mechanisms and the ability to use ACE2 receptors from additional species. *Immunity* **54**, 1611-1621 e1615, doi:10.1016/j.immuni.2021.06.003 (2021).

34 Yu, J. *et al.* Neutralization of the SARS-CoV-2 Omicron BA.1 and BA.2 Variants. *N Engl J Med* **386**, 1579-1580, doi:10.1056/NEJMc2201849 (2022).

35 Wrapp, D. *et al.* Cryo-EM structure of the 2019-nCoV spike in the prefusion conformation. *Science* **367**, 1260-1263, doi:10.1126/science.abb2507 (2020).

36 Krissinel, E. & Henrick, K. Inference of macromolecular assemblies from crystalline state. *J Mol Biol* **372**, 774-797, doi:10.1016/j.jmb.2007.05.022 (2007).

37 Cerutti, G. *et al.* Structural basis for accommodation of emerging B.1.351 and B.1.1.7 variants by two potent SARS-CoV-2 neutralizing antibodies. *Structure* **29**, 655-663 e654, doi:10.1016/j.str.2021.05.014 (2021).

Figure legends

Fig. 1 | Prevalence of SARS-CoV-2 Omicron subvariants. a, Frequencies of BA.1, BA.1.1, BA.2, BA.2.12.1, and BA.4/5 deposited in GISAID. The value in the upper right corner of each box denotes the cumulative number of sequences for all circulating viruses in the denoted time period. **b**, Unrooted phylogenetic tree of Omicron and its subvariants along with other major SARS-CoV-2 variants. The scale bar indicates the genetic distance. **c**, Key spike mutations found in BA.2, BA.2.12.1, BA.4, and BA.5. Del, deletion.

Fig. 2 | Resistance of Omicron subvariants to neutralization by monoclonal antibodies. a, Neutralization of D614G and Omicron subvariants by RBD- and NTD-directed mAbs. Values above the limit of detection of 10 μg/mL (dotted line) are arbitrarily plotted to allow for visualization of each sample. **b**, Fold change in IC_{50} values of point mutants relative to D614G or BA.2, with resistance colored red and sensitization colored green. **c**, Location of F486V, L452R/Q, and R493Q on D614G RBD, with the color indicating the per residue frequency recognized by SARS-CoV-2 neutralizing antibodies. Modeling of L452R/Q (**d**) and F486V (**e**) affect class 2 mAb neutralization. The clashes are shown in red plates; the hydrogen bonds are shown in dark dashed lines. The results shown in **a** and **b** are representative of those obtained in two independent experiments.

Fig. 3 | Affinity of the spike proteins of SARS-CoV-2 Omicron subvariants to hACE2. a, Binding affinities of Omicron subvariant S2P spike proteins to hACE2 as measured by SPR. **b**, Sensitivity of pseudotyped Omicron subvariants and the individual mutations in the background of BA.2 to hACE2 inhibition. The hACE2 concentrations resulting in 50% inhibition of infectivity (IC_{50}) are presented. Data are shown as mean ± standard error of mean (SEM) for three technical replicates. **c**, In silico analysis for how R493Q and F486V affect hACE2 binding. The hACE2 surface is shown with charge potential, with red and blue representing negative and positive charges, respectively. Omicron BA.1 RBD in complex with hACE2 was downloaded from PDB 7U0N, and the ligand-free BA.2 RBD was downloaded from PDB 7UB0. The results shown in **a** and **b** are representative of those obtained in two independent experiments.

Fig. 4 | BA.2.12.1 and BA.4/5 exhibit greater serum neutralization resistance profiles relative to BA.2. a, Neutralization of pseudotyped D614G and Omicron subvariants by sera from 4 different clinical cohorts. **b**, Fold change in geometric mean ID_{50} titers of boosted vaccinee sera

relative to D614G and BA.2, with resistance colored red and sensitization colored green. **c**, Serum neutralization of BA.2 pseudoviruses containing single mutations found within BA.2.12.1 and BA.4/5. **d**, Antigenic map based on the neutralization data of boosted vaccinee sera. SARS-CoV-2 variants are shown as colored circles and sera are shown as grey squares. The x-, y-, and z-axis represent antigenic units (AU) with one grid corresponding to a two-fold serum dilution of the neutralization titer. An interactive map is available online (https://figshare.com/articles/media/OmicronAntigenicMap/19854046). The map orientation within the x-, y-, and z-axis is free to rotate. For all the panels in **a** and **c**, values above the symbols denote the geometric mean ID_{50} values and values on the lower left show the sample size (n) for each group. *P* values were determined by using two-tailed Wilcoxon matched-pairs signed-rank tests. The results shown are representative of those obtained in two independent experiments.

Methods

Data reporting

No statistical methods were used to predetermine sample size. The experiments were not randomized and the investigators were not blinded to allocation during experiments and outcome assessment.

Serum samples

Sera from individuals who received three doses of the mRNA-1273 or BNT162b2 vaccine were collected at Columbia University Irving Medical Center. Sera from individuals who were infected by non-Omicron variants of SARS-CoV-2 in addition to vaccination were collected from January 2021 to September 2021 at Columbia University Irving Medical Center or at the Hackensack Meridian Center for Discovery and Innovation (CDI). Sera from individuals who were infected by Omicron (BA.1 or BA.2) following vaccinations were collected from December 2021 to May 2022 at Columbia University Irving Medical Center. All samples were confirmed for prior SARS-CoV-2 infection status by anti-nucleoprotein (NP) ELISA. All collections were conducted under protocols reviewed and approved by the Institutional Review Board of Columbia University or the Hackensack Meridian Center for Discovery and Innovation. All participants provided written informed consent. Clinical information on the different cohorts of study subjects is provided in Extended Data Table 2.

Monoclonal antibodies

Antibodies were expressed as previously described[17]. Heavy chain variable (VH) and light chain variable (VL) genes for each antibody were synthesized (GenScript), then transfected into Expi293 cells (Thermo Fisher Scientific), and purified from the supernatant by affinity purification using rProtein A Sepharose (GE). REGN10987, REGN10933, COV2-2196, and COV2-2130 were provided by Regeneron Pharmaceuticals; Brii-196 and Brii-198 were provided by Brii Biosciences; CB6 was provided by B. Zhang and P. Kwong (NIH); and ZCB11 was provided by Z. Chen (HKU).

Cell lines

Expi293 cells were obtained from Thermo Fisher Scientific (A14527); Vero-E6 cells were obtained from the ATCC (CRL-1586); HEK293T cells were obtained from the ATCC (CRL-3216). Cells were purchased from authenticated vendors and morphology was confirmed visually before use. All cell lines tested mycoplasma negative.

Variant SARS-CoV-2 spike plasmid construction

BA.1, BA.1.1, and BA.2 spike-expressing plasmids were generated as previously described[23,26]. Plasmids encoding the BA.2.12.1 and BA.4/5 spikes, as well as the individual and double mutations found in BA.2.12.1 and BA.4/5, were generated using the QuikChange II XL site-directed mutagenesis kit according to the manufacturer's instructions (Agilent). To make the constructs for expression of stabilized soluble S2P spike trimer proteins, 2P substitutions (K986P and V987P) and a "GSAS" substitution of the furin cleavage site (682-685aa in WA1) were introduced into the spike-expressing plasmids[35], and then the ectodomain (1-1208aa in WA1) of the spike was fused with a C-terminal 8x His-tag and cloned into the **paH** vector. All constructs were confirmed by Sanger sequencing.

Expression and purification of SARS-CoV-2 S2P spike proteins

SARS-CoV-2 S2P spike trimer proteins of the D614G and Omicron subvariants were generated by transfecting Expi293 cells with the S2P spike trimer-expressing constructs using 1 mg mL^{-1} polyethylenimine (PEI) and then purifying from the supernatants five days post-transfection using Ni-NTA resin (Invitrogen) according to the manufacturer's instructions[17].

Surface plasmon resonance

Surface plasmon resonance (SPR) binding assays for hACE2 binding to SARS-CoV-2 S2P spike were performed using a Biacore T200 biosensor equipped with a Series S CM5 chip (Cytiva), in a running buffer of 10 mM HEPES pH 7.4, 150 mM NaCl, 3 mM EDTA, 0.05% P-20 (Cytiva) at 25 °C. Spike proteins were captured through their C-terminal His-tag over an anti-His antibody surface. These surfaces were generated using the His-capture kit (Cytiva) according to the manufacturer's instructions, resulting in approximately 10,000 RU of anti-His antibody over each surface. An anti-His antibody surface without antigen was used as a reference flow cell to remove bulk shift changes from the binding signal.

Binding of human ACE2-Fc protein (Sino Biological) was tested using a three-fold dilution series with concentrations ranging from 2.46 nM to 200 nM. The association and dissociation rates were each monitored for 60 s and 300 s respectively, at 30 µL/min. The bound spike/ACE2 complex was regenerated from the anti-His antibody surface using 10 mM glycine pH 1.5. Blank buffer cycles were performed by injecting running buffer instead of human ACE2-Fc to remove systematic noise from the binding signal. The resulting data was processed and fit to a 1:1 binding model using Biacore Evaluation Software.

Pseudovirus production

Pseudoviruses were produced in the vesicular stomatitis virus (VSV) background, in which the native glycoprotein was replaced by that of SARS-CoV-2 and its variants, as previously described[17]. In brief, HEK293T cells were transfected with a spike expression construct with 1 mg mL^{-1} polyethylenimine (PEI) and cultured overnight at 37 °C under 5% CO_2, and then infected with VSV-G pseudotyped ΔG-luciferase (G*ΔG-luciferase, Kerafast) one day post-transfection. After 2 h of infection, cells were washed three times, changed to fresh medium, and then cultured for approximately another 24 h before the supernatants were collected, clarified by centrifugation, and aliquoted and stored at -80 °C for further use.

Pseudovirus neutralization assay

All viruses were first titrated to normalize the viral input between assays. Heat-inactivated sera or antibodies were first serially diluted (five-fold) in medium in 96-well plates in triplicate, starting at 1:100 dilution for sera and 10 µg mL^{-1} for antibodies. Pseudoviruses were then added and the virus–sample mixture was incubated at 37 °C for 1 h. Vero-E6 cells were then added at a density of 3×10^4 cells per well and the plates were incubated at 37 °C for approximately 10 h. Luciferase activity was quantified using the Luciferase Assay System (Promega) according to the manufacturer's instructions using SoftMax Pro v.7.0.2 (Molecular Devices). Neutralization curves and IC_{50} values were derived by fitting a nonlinear five-parameter dose-response curve to the data in GraphPad Prism v.9.2.

Authentic virus neutralization assay

418 The SARS-CoV-2 viruses hCoV-19/USA/CO-CDPHE-2102544747/2021 (BA.2) and hCoV-
419 19/USA/MD-HP30386/2022 (BA.4) were obtained from BEI Resources (NIAID, NIH) and
420 propagated by passaging in Vero-E6 cells. Virus infectious titers were determined by an end-point
421 dilution and cytopathogenic effect assay on Vero-E6 cells as previously described[17].
422
423 An end-point dilution microplate neutralization assay was performed to measure the neutralization
424 activity of sera from vaccinated and boosted individuals as well as of purified monoclonal
425 antibodies. In brief, serum samples were subjected to successive five-fold dilutions starting from
426 1:100. Monoclonal antibodies were serially diluted (five-fold) starting at 5 μg/ml. Triplicates of
427 each dilution were incubated with SARS-CoV-2 at a multiplicity of infection of 0.1 in EMEM
428 with 7.5% inactivated fetal calf serum for 1 h at 37 °C. After incubation, the virus–antibody
429 mixture was transferred onto a monolayer of Vero-E6 cells grown overnight. The cells were
430 incubated with the mixture for around 70 h. Cytopathogenic effects of viral infection were visually
431 scored for each well in a blinded manner by two independent observers. The results were then
432 converted into the percentage of neutralization at a given sample dilution or monoclonal antibody
433 concentration, and the data (mean ± SEM) were plotted using a five-parameter dose-response curve
434 in GraphPad Prism v.9.2.
435
436 **Antibody targeting frequency and mutagenesis analysis for RBD**
437 The SARS-CoV-2 spike structure (6ZGE) used for displaying epitope footprints was downloaded
438 from the Protein Data Bank (PDB). Epitope residues were identified using PISA[36] with default
439 parameters, and the RBD residues with non-zero buried accessible surface area were considered
440 epitope residues. For each residue within the RBD, the frequency of antibody recognition was
441 calculated as the number of contact antibodies[37]. The structures of antibody-spike complexes for
442 modeling were also obtained from PDB (7L5B (2-15), 6XDG (REGN10933), and 7KMG (LY-
443 CoV555)). Omicron BA.1 RB D in complex with hACE2 was downloaded from PDB 7U0N, and
444 the ligand-free BA.2 RBD was downloaded from PDB 7UB0. PyMOL v.2.3.2 was used to perform
445 mutagenesis and to generate structural plots (Schrödinger, LLC).
446
447 **Antigenic cartography**

448 The antigenic distances between SARS-CoV-2 variants were approximated by incorporating the
449 neutralization potency of each serum sample into a previously described antigenic cartography
450 approach[27]. The map was generated by the Racmacs package (https://acorg.github.io/Racmacs/,
451 version 1.1.4) in R with the optimization steps set to 2000, and with the minimum column basis
452 parameter set to “none”.
453

Acknowledgements

This study was supported by funding from the Gates Foundation, JPB Foundation, Andrew and Peggy Cherng, Samuel Yin, Carol Ludwig, David and Roger Wu, Regeneron Pharmaceuticals, and the NIH SARS-CoV-2 Assessment of Viral Evolution (SAVE) Program. We acknowledge David S. Perlin for providing serum samples from a few COVID-19 patients. We thank all who contributed their data to GISIAD.

Author contributions

D.D.H. and L.L. conceived this project. Q.W. and L.L. conducted pseudovirus neutralization experiments and purified SARS-CoV-2 spike proteins. Y.G. and Z.S. conducted bioinformatic analyses. Q.W., L.L., and S.I. constructed the spike expression plasmids. Q.W. managed the project. J.Y. M.W., and Z.C. expressed and purified antibodies. L.L. and Z.L. performed surface plasmon resonance (SPR) assay. M.T.Y., M.E.S., J.Y.C., A.D.B. J.G.S., N.N., and K.M. provided clinical samples. H.M. aided sample collections. M.S.N. and Y.H. performed infectious SARS-CoV-2 neutralization assays. D.D.H. and L.L. directed and supervised the project. Q.W., Y.G., L.L., and D.D.H. analyzed the results and wrote the manuscript.

Competing interests

S.I, J.Y., Y.H., L.L., and D.D.H. are inventors on patent applications (WO2021236998) or provisional patent applications (63/271,627) filed by Columbia University for a number of SARS-CoV-2 neutralizing antibodies described in this manuscript. Both sets of applications are under review. D.D.H. is a co-founder of TaiMed Biologics and RenBio, consultant to WuXi Biologics and Brii Biosciences, and board director for Vicarious Surgical.

Additional information

Correspondence and requests for materials should be addressed to L.L. or D. D. H.

Reprints and permissions information is available at www.nature.com/reprints.

Data availability

All data are provided in the manuscript. Materials in this study will be made available under an appropriate Materials Transfer Agreement. Sequences for Omicron prevalence analysis were

485 downloaded from GISAID (https://www.gisaid.org/). The structures used for analysis in this study
486 are available from PDB under IDs 6ZGE, 7L5B, 6XDG, 7U0N, 7UB0 and 7KMG. The interactive
487 antigenic map based on the neutralization data of boosted vaccine sera in Figure 4d is available
488 online (https://figshare.com/articles/media/OmicronAntigenicMap/19854046).
489

Extended Data Figure Legends

Extended Data Fig. 1 | Pseudovirus (a) and authentic virus (b) neutralization curves of D614G and Omicron subvariants by monoclonal antibodies. Data are shown as mean ± SEM from three technical replicates and representative of those obtained in two independent experiments.

Extended Data Fig. 2 | Neutralization IC_{50} values for indicated pseudoviruses (a) and authentic viruses (b) by monoclonal antibodies. Data are representative of those obtained in two independent experiments.

Extended Data Fig. 3 | Pseudovirus neutralization curves for monoclonal antibodies against individual SARS-CoV-2 mutations in the background of D614G. Data are shown as mean ± SEM from three technical replicates and representative of those obtained in two independent experiments.

Extended Data Fig. 4 | Pseudovirus neutralization curves for monoclonal antibodies against individual SARS-CoV-2 mutations in the background of BA.2. Data are shown as mean ± SEM from three technical replicates and representative of those obtained in two independent experiments.

Extended Data Fig. 5 | Pseudovirus neutralization IC_{50} values for monoclonal antibodies. IC_{50} values of **a**, D614G carrying individual mutations; **b**, BA.2 carrying individual mutations. Data are representative of those obtained in two independent experiments.

Extended Data Fig. 6 | Neutralization curves of serum against D614G and Omicron subvariants. Neutralization by **a**, boosted vaccinee sera on pseudoviruses. **b**, non-Omicron infection & vaccination sera on pseudoviruses. **c**, BA.1 breakthrough sera on pseudoviruses. **d**, BA.2 breakthrough sera on pseudoviruses. **e**, boosted vaccinee sera on authentic viruses. **f**, Neutralization ID_{50} titers of authentic BA.2 and BA.4 by boosted vaccinee sera. Values above the symbols denote the geometric mean ID_{50} values and values on the lower left show the sample size

(n). *P* values were determined by using two-tailed Wilcoxon matched-pairs signed-rank tests. Error bars in **a**, **b**, **c**, **d**, and **e** denote mean ± SEM for three technical replicates. All data are representative of those obtained in two independent experiments.

Extended Data Fig. 7 | Pseudovirus neutralization curves of serum against BA.2 and BA.2 pseudovirus carrying individual mutations. Neutralization by **a**, boosted vaccinee sera. **b**, non-Omicron infection & vaccination sera. **c**, BA.1 breakthrough sera. **d**, BA.2 breakthrough sera. Error bars denote mean ± SEM for three technical replicates. Data are representative of those obtained in two independent experiments.

Extended Data Table 1 | Mutation frequencies at position F486 within different SARS-CoV-2 variants.

Extended Data Table 2 | Demographics on the clinical cohorts.

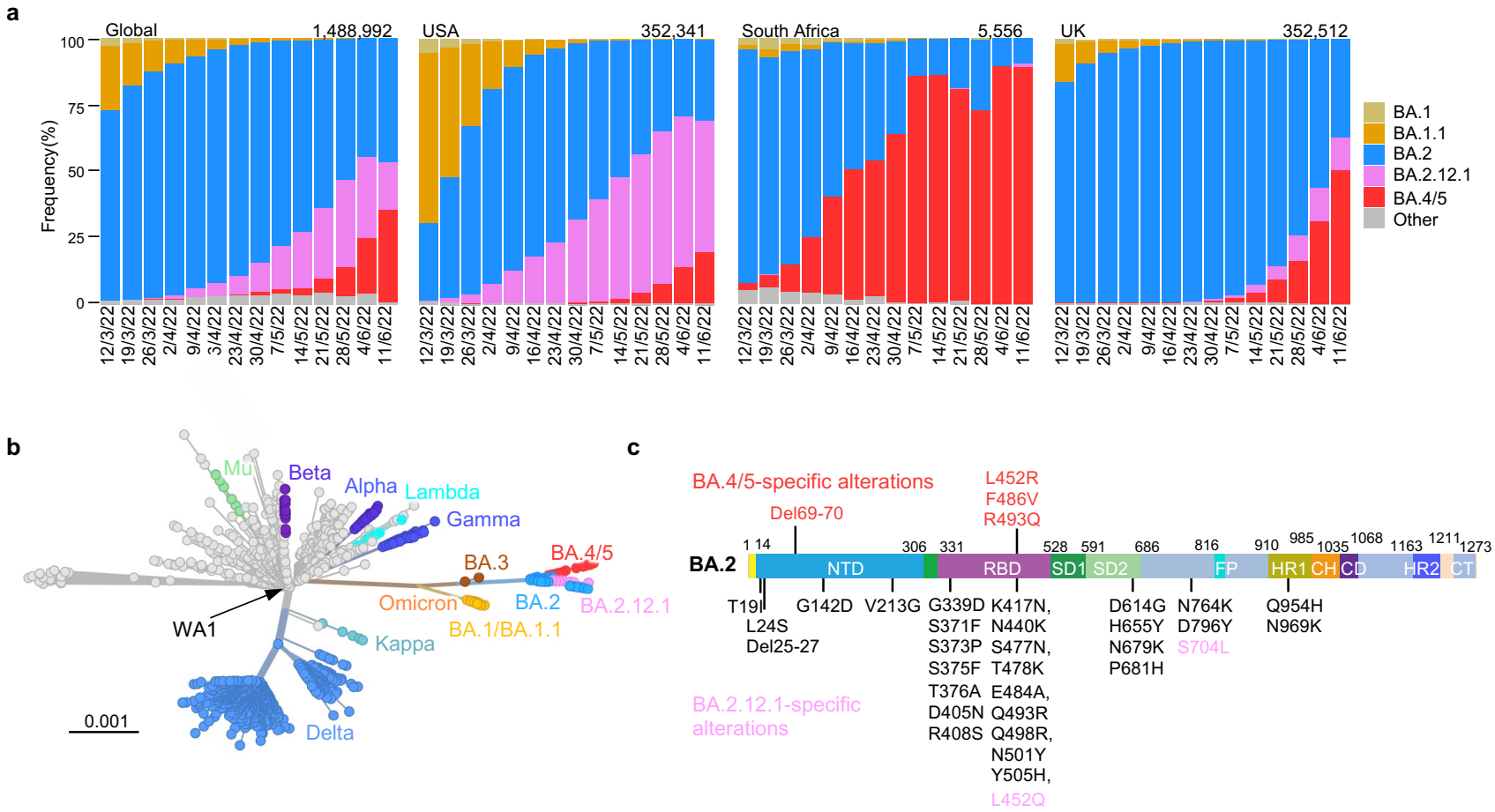
a
Global
1,488,992
USA
352,341
South Africa
5,556
UK
352,512
Frequency(%)
100
75
50
25
0
12/3/22
19/3/22
26/3/22
2/4/22
9/4/22
3/4/22
16/4/22
23/4/22
30/4/22
7/5/22
14/5/22
21/5/22
28/5/22
4/6/22
11/6/22
BA.1
BA.1.1
BA.2
BA.2.12.1
BA.4/5
Other
b
Mu
Beta
Alpha
Lambda
Gamma
BA.3
BA.4/5
Omicron
BA.2
BA.2.12.1
WA1
BA.1/BA.1.1
Kappa
Delta
0.001
c
BA.4/5-specific alterations
Del69-70
L452R
F486V
R493Q
BA.2
1 14
306
331
528
591
686
816
910
985
1035
1068
1163
1211
1273
NTD
RBD
SD1
SD2
FP
HR1
CH
CD
HR2
CT
T19I
L24S
Del25-27
G142D
V213G
G339D
S371F
S373P
S375F
T376A
D405N
R408S
K417N,
N440K
S477N,
T478K
E484A,
Q493R
Q498R,
N501Y
Y505H,
L452Q
D614G
H655Y
N679K
P681H
N764K
D796Y
S704L
Q954H
N969K
BA.2.12.1-specific
alterations

a

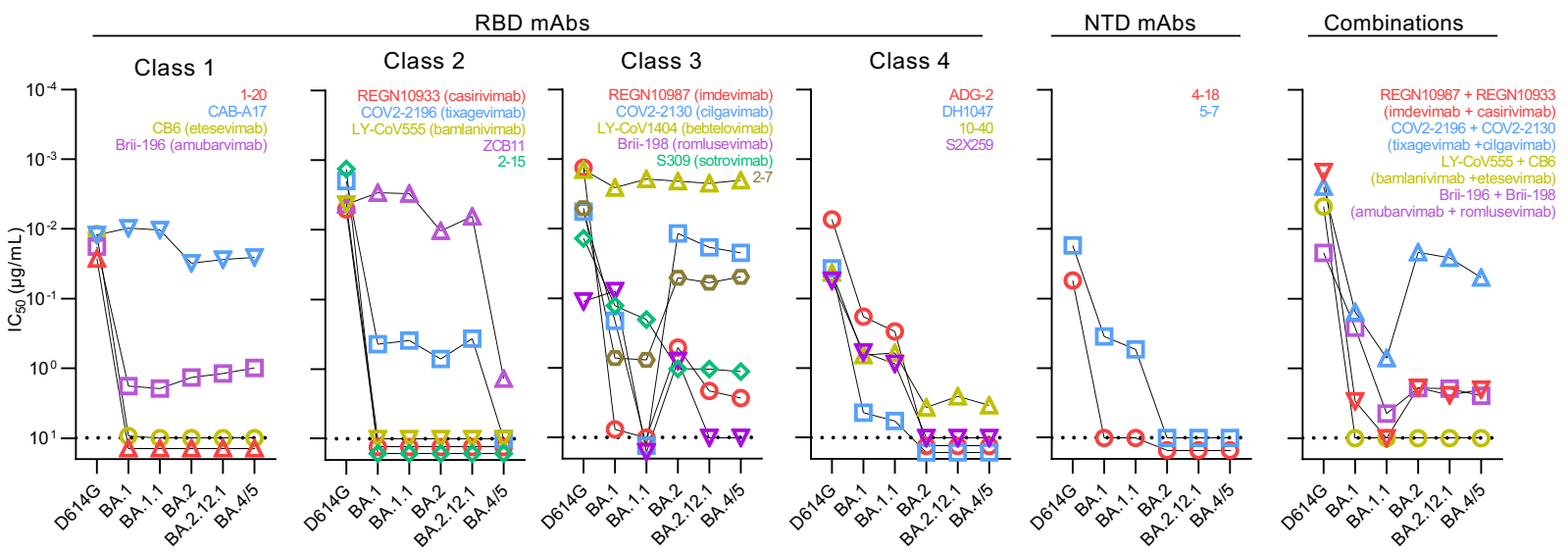

b

Fold change in IC50		RBD mAbs																			NTD mAbs		Combinations			
		Class 1				Class 2					Class 3						Class 4									
		1-20	CAB-A17	CB6	Brii-196	REGN10933	COV2-2196	LY-CoV555	ZCB11	2-15	REGN10987	COV2-2130	LY-CoV1404	Brii-198	S309	2-7	ADG-2	DH1047	10-40	S2X259	4-18	5-7	REGN10987 + REGN10933	COV2-2196 + COV2-2130	LY-CoV555 + CB6	Brii-196 + Brii-198
Compared with D614G	D614G-Del69-70	1.3	1.1	1.3	-1.3	-1.0	-1.0	2.0	-1.4	1.3	-1.3	-2.1	-1.3	-1.1	-2.0	-1.0	-1.6	-1.3	-1.7	-1.6	-1.1	-4.6	-1.7	-1.5	-1.1	-1.0
	D614G-L452M	1.5	-1.0	1.5	-1.0	<-1.9	-1.0	-1.8	-1.0	-0.9	-1.5	-1.7	-1.0	-6.9	-2.0	-1.0	-1.5	1.1	1.3	-1.0	-1.1	-1.3	-1.5	-1.1	-1.1	-1.0
	D614G-L452R	-1.2	-1.3	-1.4	-1.5	<-2.0	-1.0	-2266	-1.1	-16	-2.1	-2.6	-1.2	-27	-1.6	-1.8	-1.3	-1.0	1.4	1.8	1.1	-1.1	-1.3	-1.0	-3.9	-1.3
	D614G-L452Q	-1.3	1.1	-1.0	-1.4	<-2.1	-1.0	-5.3	-1.0	-11	-3.7	-3.8	-1.5	-18	-2.7	-2.2	-1.5	-1.5	-1.8	-1.7	-2.0	-1.6	-2.5	-1.7	-3.0	-1.9
	D614G-F486V	-1.5	-1.2	-8.1	-14	<-10000	<-272	-886	-712	-24	-1.1	-1.4	-1.3	-1.4	-1.0	-0.8	-1.4	1.1	-1.7	-2.2	1.1	-1.0	-4.8	-10	-154	-11
	D614G-S704L	1.3	-1.0	-1.6	-1.2	-1.0	-1.0	-1.0	-1.0	-1.3	-1.6	-3.0	1.2	-1.5	-2.7	-1.6	-1.3	-1.7	-1.9	-1.9	-1.9	-1.1	-1.8	-1.5	-1.5	-1.2
	D614G-L452Q/S704L	-1.3	-1.3	-1.9	-1.6	<-7.2	<-1.5	-8.5	-2.8	-32	-4.2	-4.9	-1.5	-48	-2.0	-3.1	-1.8	-1.4	-2.4	-3.0	-2.0	-2.1	-2.4	-2.1	-3.6	-2.2
Compared with BA.2	BA.2-Del69-70	-1.0	-1.5	-1.0	-2.1	-1.0	1.3	-1.0	1.1	-1.0	1.7	1.1	-1.2	1.6	-1.2	-1.0	-1.0	-1.0	<-2.1	-1.0	-1.0	-1.0	-1.5	-1.0	-1.0	1.2
	BA.2-L452M	-1.0	-1.4	-1.0	1.5	-1.0	1.1	-1.0	-1.5	-1.0	-2.2	-2.8	-1.4	<-16	-1.4	-1.3	-1.0	-1.0	1.1	-1.0	-1.0	-1.0	1.2	-1.0	-1.0	1.4
	BA.2-L452R	-1.0	-1.8	-1.0	-5.1	-1.0	-1.2	-1.0	-1.8	-1.0	-5.7	-4.6	-1.1	<-16	-2.6	1.2	-1.0	-1.0	<-2.1	-1.0	-1.0	-1.0	1.3	-1.8	-1.0	<-6.3
	BA.2-L452Q	-1.0	-1.3	-1.0	-1.3	-1.0	1.6	-1.0	1.5	-1.0	-1.8	-1.9	-1.4	<-16	-1.4	-1.6	-1.0	-1.0	<-2.1	-1.0	-1.0	-1.0	-3.2	-1.5	-1.0	-3.5
	BA.2-F486V	-1.0	-8.6	-1.0	<-7.5	1.0	<-9.4	-1.0	<-2182	-1.0	-3.4	1.1	1.1	-1.4	-1.0	-1.7	-1.0	-1.0	-1.2	-1.0	-1.0	-1.0	-5.0	-1.2	-1.0	-3.4
	BA.2-R493Q	>5.0	2.7	-1.0	41.0	>10	22	-1.0	4.6	-1.0	1.1	-1.7	-1.7	-1.7	-1.2	-1.5	-1.0	-1.0	1.6	-1.0	-1.0	-1.0	2.3	1.8	-1.0	76
	BA.2-S704L	-1.0	-1.2	-1.0	-1.1	-1.0	1.5	-1.0	1.2	-1.0	1.9	-1.1	-1.3	-1.1	-1.4	1.1	-1.0	-1.0	1.9	-1.0	-1.0	-1.0	1.2	1.7	-1.0	2.0
	BA.2-F486V/R493Q	-1.0	1.3	-1.0	3.4	-1.0	<-9.4	-1.0	-1694	-1.0	1.5	1.7	1.6	2.2	1.9	1.4	-1.0	-1.0	1.8	-1.0	-1.0	-1.0	1.7	1.1	-1.0	2.7

>10	>3	<-3	<-10	<-100	<-1000

c

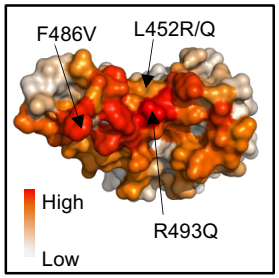

d

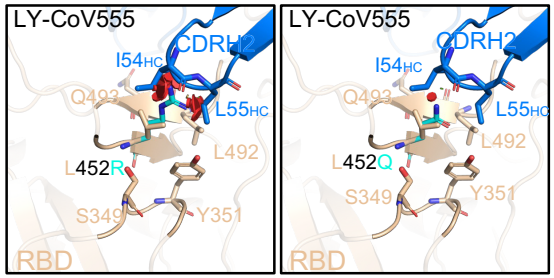

e

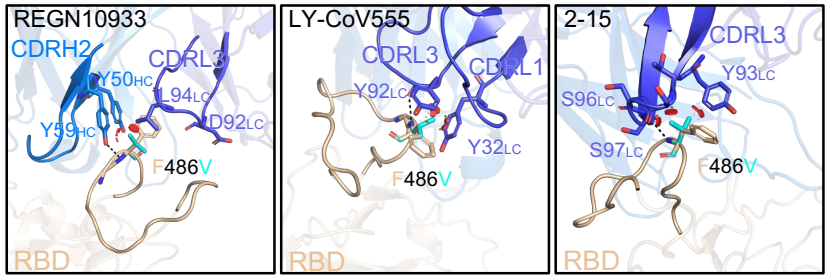

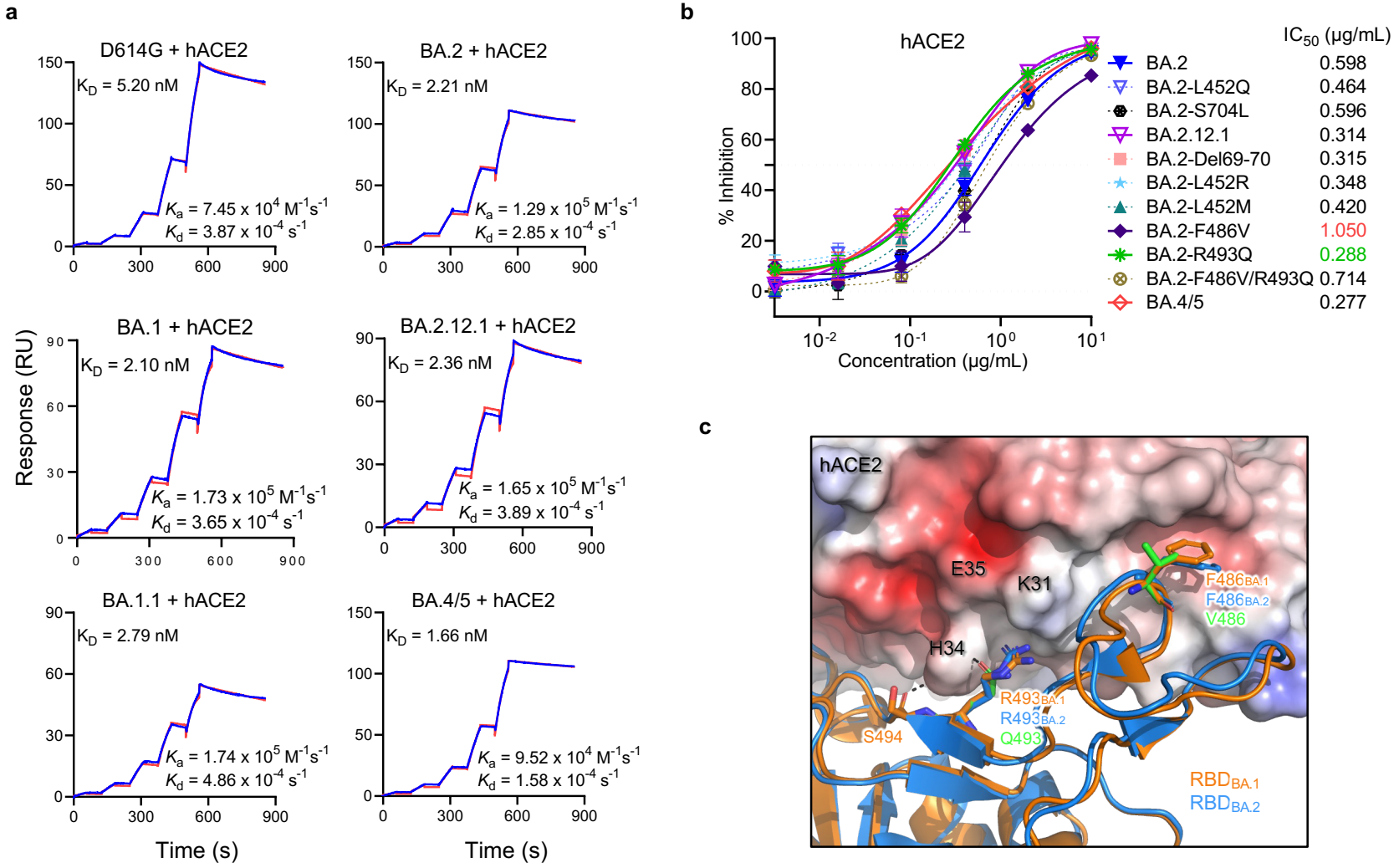
a
D614G + hACE2
K_D = 5.20 nM
K_a = 7.45 x 10^4 M^-1s^-1
K_d = 3.87 x 10^-4 s^-1
BA.2 + hACE2
K_D = 2.21 nM
K_a = 1.29 x 10^5 M^-1s^-1
K_d = 2.85 x 10^-4 s^-1
BA.1 + hACE2
K_D = 2.10 nM
K_a = 1.73 x 10^5 M^-1s^-1
K_d = 3.65 x 10^-4 s^-1
BA.2.12.1 + hACE2
K_D = 2.36 nM
K_a = 1.65 x 10^5 M^-1s^-1
K_d = 3.89 x 10^-4 s^-1
BA.1.1 + hACE2
K_D = 2.79 nM
K_a = 1.74 x 10^5 M^-1s^-1
K_d = 4.86 x 10^-4 s^-1
BA.4/5 + hACE2
K_D = 1.66 nM
K_a = 9.52 x 10^4 M^-1s^-1
K_d = 1.58 x 10^-4 s^-1
Response (RU)
Time (s)
Time (s)
b
hACE2
% Inhibition
Concentration (μg/mL)
IC50 (μg/mL)
BA.2 0.598
BA.2-L452Q 0.464
BA.2-S704L 0.596
BA.2.12.1 0.314
BA.2-Del69-70 0.315
BA.2-L452R 0.348
BA.2-L452M 0.420
BA.2-F486V 1.050
BA.2-R493Q 0.288
BA.2-F486V/R493Q 0.714
BA.4/5 0.277
c
hACE2
E35
K31
H34
S494
F486BA.1
F486BA.2
V486
R493BA.1
R493BA.2
Q493
RBDBA.1
RBDBA.2

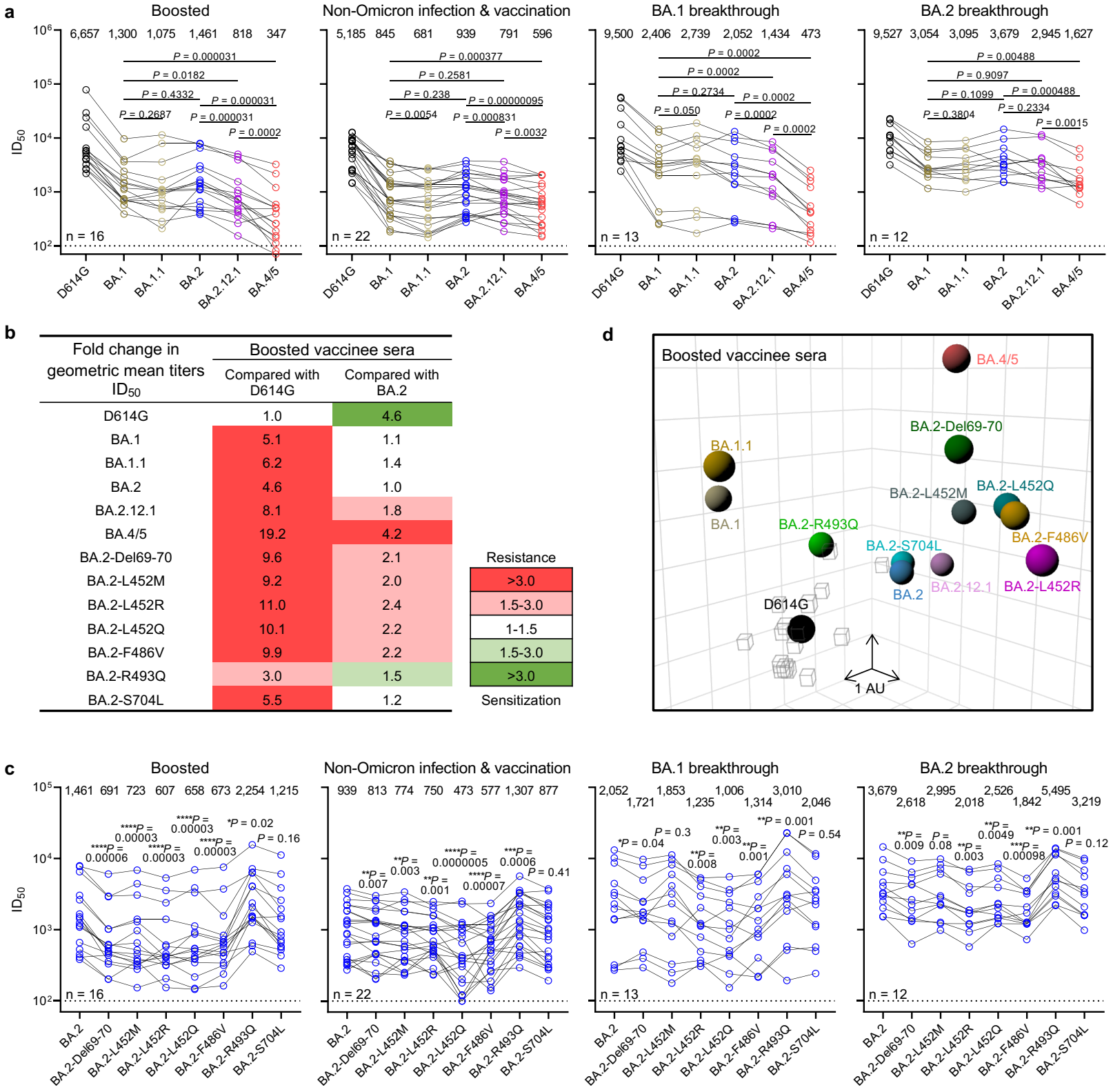
a
Boosted
Non-Omicron infection & vaccination
BA.1 breakthrough
BA.2 breakthrough
ID50
n = 16
n = 22
n = 13
n = 12
D614G
BA.1
BA.1.1
BA.2
BA.2.12.1
BA.4/5
b
Fold change in geometric mean titers ID50
Boosted vaccinee sera
Compared with D614G
Compared with BA.2
D614G 1.0 4.6
BA.1 5.1 1.1
BA.1.1 6.2 1.4
BA.2 4.6 1.0
BA.2.12.1 8.1 1.8
BA.4/5 19.2 4.2
BA.2-Del69-70 9.6 2.1
BA.2-L452M 9.2 2.0
BA.2-L452R 11.0 2.4
BA.2-L452Q 10.1 2.2
BA.2-F486V 9.9 2.2
BA.2-R493Q 3.0 1.5
BA.2-S704L 5.5 1.2
Resistance
>3.0
1.5-3.0
1-1.5
1.5-3.0
>3.0
Sensitization
d
Boosted vaccinee sera
BA.4/5
BA.2-Del69-70
BA.1.1
BA.2-L452M
BA.2-L452Q
BA.1
BA.2-R493Q
BA.2-F486V
BA.2-S704L
BA.2
BA.2.12.1
BA.2-L452R
D614G
1 AU
c
Boosted
Non-Omicron infection & vaccination
BA.1 breakthrough
BA.2 breakthrough
ID50
n = 16
n = 22
n = 13
n = 12
BA.2
BA.2-Del69-70
BA.2-L452M
BA.2-L452R
BA.2-L452Q
BA.2-F486V
BA.2-R493Q
BA.2-S704L